ISSN 1029-9599, Physical Mesomechanics, 2023, Vol. 26, No. 2, pp. 196–208. © Pleiades Publishing, Ltd., 2023.
Russian Text © The Author(s), 2022, published in Fizicheskaya Mezomekhanika, 2022, Vol. 25, No. 6, pp. 106–119.

Production of Biodegradable Metal Foams by Powder Metallurgy Method

G. Demir[1], D. Akyurek[2], A. Hassoun[2], and I. Mutlu[2]*

[1] *Department of Molecular Biology and Genetics, Bilecik Seyh Edebali University, Bilecik, 11230 Turkey*
[2] *Metallurgical and Materials Engineering Department, Istanbul University-Cerrahpasa, Istanbul, 34320 Turkey*
* *e-mail: imutlu@istanbul.edu.tr, imutlu@iuc.edu.tr*

Received February 12, 2022; revised May 21, 2022; accepted June 03, 2022

Abstract—In this study, highly porous biocompatible and biodegradable zinc, iron and magnesium alloy foams were fabricated for temporary implant and scaffold applications. Specimens with open porous structure were fabricated by powder metallurgy based space holder method. Mg, Fe and Zn are the main bioabsorable metals. Mg alloys biodegrade too fast with H_2 evolution. Biodegradation rate of Fe alloys is too slow, and by-products remain inside the body. Zn alloys show biodegradation rates in the middle of Mg and Fe alloys, and their biodegradation by-products are bioresorbable. Here several Fe, Zn, and Mg alloys were manufactured, and comparatively characterized. Effects of alloying elements on biodegradation, corrosion and mechanical properties were investigated separately. As the mechanical properties of temporary implants must decrease slowly, the variation of mechanical properties with time in the foams was investigated. Corrosion performance was tested in simulated body fluid. Biodegradation rate was investigated by using weight loss and metal ion release measurements. The corrosion and biodegradation rates of Zn specimens were lower than in Mg specimens and higher than in Fe specimens. Fe^{2+}, Zn^{2+} and Mg^{2+} ion release amounts were lower than the upper limit for humans.

Keywords: corrosion, metal foam, biodegradation, space holder, powder metallurgy, temporary implant

DOI: 10.1134/S102995992302008X

1. INTRODUCTION

Biomaterial can be described as a man-made nonviable material used to produce medical devices to replace parts of a living body or to function in contact with living tissue. In general, an implant is a medical device fabricated from biomaterials in order to replace a missing body part, to support a damaged body part, or to enhance a body part. Conventional bioinert metals (CoCr alloys, austenitic stainless steels, Ti alloys) are used to manufacture hard tissue implants due to their high corrosion properties and suitable elastic modulus close to bone. In bioinert metals, there is no chemical bonding and there is minimal interaction with the body. Current hard tissue implants manufactured by using bioinert metals are aimed to stay in the body permanently [1–3]. Highly prous bioabsorbable scaffolds are used in tissue engineering. A bioabsorbable scaffold provides mechanical support for living cells and determines the shape of tissues. Such a scaffold allows the transportation of body fluids through open pores and provides tissue growth. Scaffold materials should have a definite biodegradation rate. Meanwhile, biodegradable metals can be used in temporary implant applications. Complete dissolution of bioabsorbable implants assists tissue healing without any residues. Permanent metallic implants show problems such as inflammation, thrombosis, and stress shielding. Moreover, permanent implants need secondary surgery [1–3].

The conventional paradigm of metallic biomaterials requires metals with high corrosion resistance. Biodegradable metals are metals expected to corrode gradually with a suitable host response. Biodegradable metals can be classified as biodegradable pure metals, biodegradable alloys, and biodegradable metal matrix composites. Polymer biomaterials have low strength and low wear resistance and release toxic reagents, while ceramic biomaterials are very brittle. Mg, Fe and Zn are three main bioabsorable metals. Mg alloys biodegrade too fast (up to 12 weeks) with H_2 evolution. The biodegradation rate of iron alloys is too slow (up to about 150 weeks), and by-pro-

ducts of Fe remain inside the body for a long time. Zn is a promising biodegradable metal along with Mg and Fe alloys. Zn alloys show biodegradation rates in the middle of Mg alloys and Fe alloys, and their by-products are bioresorbable.

Mg alloys can be used as a material in temporary implant manufacturing. In general, the Mg content in bones is about 25–40 g. Mg is important for enzyme reactions. The high corrosion rate of Mg alloys is attributed to its low standard electrode potential. The corrosion products of Mg can be metabolized or digested. In addition, Mg alloys can stimulate bone formation, which is important in bone healing. The mechanical properties of Mg are very low for implant applications but eliminate the possible toxic effects of alloying elements. The biodegradation rate of Mg alloys is very high. Moreover, Mg alloys produce hydrogen during biodegradation.

Fe alloys are in general biodegradable and nontoxic. Fe alloys show radioopacity, so that markers to make a coronary stent visible by fluoroscopy are not required. Fe is essential for some enzymes. The corrosion rate of Fe-based alloys is very low, which is not suitable for temporary implant applications. Although the biodegradation products of Fe alloys are biocompatible, they can lead to delays of oxygen transport important for biodegradation of Fe. So, the biodegradation of Fe is too slow compared to the tissue healing time. Moreover, Fe alloys suffer from harmful corrosion by-products (iron oxides with high volume). In stent applications, the formation of iron oxide by-products decreases the cross section of the vein. Pure Fe has advantages over pure Mg alloys and pure Zn alloys for stent applications in terms of mechanical properties [1–3].

Compared with biodegradable Mg and Fe alloys, interest in biocompatible and biodegradable Zn alloys for temporary implant applications is rather recent. Zn alloys show low melting temperatures and fluidity, which make them suitable for casting. Nowadays zinc has been studied as a biodegradable material. Since the standard electrode potential of Zn is lower than that of Fe and higher than that of Mg, Zn alloys can have appropriate biodegradation rate [4]. Corrosion of zinc does not produce hydrogen due to its high hydrogen over-potential. Zinc has important physiological functions, participating in nucleic acid metabolism and stimulating bone formation. Zinc is not toxic at low levels. The daily intake of zinc is about 40 mg. Zn alloys have good machinability, low melting point, and low oxygen reactivity. However, zinc shows low strength and low plastic deformation. The development of Zn alloys with high strength and ductility is one of the aims of scientists. Low fatigue properties, recrystallization at low temperatures, and susceptibility to aging may lead to failure of Zn-based implants in storage [4–8].

Porous open-cell foams can be manufactured by powder metallurgy. There are no solubility limitations in powder metallurgy as compared with casting. The repeatability of the powder metallurgy method is superior [9–18]. Sadighikia et al. [9] manufactured Zn foams with interconnected porous open-cellular microstructure by using the powder metallurgy based space holder technique. They used carbamide as a pore former. Azizi et al. [10] produced Zn-Al-Cu based alloy by using powder metallurgy. Berent et al [13] studied cast Zn-Al-Si alloy specimens. Alloys based on the eutectic Zn-Al composition were considered as they show a higher melting temperature, lower corrosion rate, and enhanced mechanical properties. The addition of Si to Zn-Al based alloys not only stops the growth of microstructural phases at the interface but also increases the mechanical properties. Kafri et al. [14] studied metallic Zn-Fe alloy for biodegradable implant applications. Iron was used as an alloying element in Zn in order to adjust the biodegradation rate due to the microgalvanic effect produced by secondary phases. Zn-Fe alloy specimens were manufactured by casting. The corrosion rate of the Zn-Fe alloy specimens was higher than that of pure Zn specimens. Francis et al. [19] studied Fe alloys for stent applications. Fe alloy based implants show strength, high corrosion rate, and suitable biocompatibility. Because of their suitable biocompatibility and suitable interaction with living tissue, Fe alloy based stents may biodegrade slowly while retaining their mechanical integrity. The potential of Fe alloys was attributed to the reduction of side effects such as inflammation and restenosis. Further research on alloy development should be performed with account for biodegradation. Orinakova et al. [20] produced iron alloy foams for orthopaedic implant applications. Highly porous iron foams were fabricated by the replication method using foamed polyurethane. Capek et al. [21] produced Fe foams with 30–80% porosity by powder metallurgy. Ammonium bicarbonate was used as a space holder.

In the present study, highly porous open-cell foams of Zn, Fe, and Mg alloys were fabricated for scaffold or temporary implant applications. Highly porous specimens with interconnected pores were obtained by the conventional powder metallurgy based space holder method. Mg, Fe and Zn are three main

bioabsorable metals. Mg alloys biodegrade too fast with H_2 evolution. The biodegradation rate of Fe alloys is too slow, and by-products of Fe remain inside the body for a long time. Zn is a promising biodegradable metal along with Mg and Fe alloys. Zn alloys show biodegradation rates in the middle of Mg and Fe alloys, and their biodegradation by-products are bioresorbable. Although there are studies on cast or powder metallurgy biodegradable Fe, Mg, and Zn alloy foams, the time variation of mechanical properties of open-cell foams has not been studied so far. Since the mechanical properties of temporary biodegradable implants must decrease slowly, the variation of mechanical properties of foams with time must be investigated. There are studies on individual Fe, Mg, and Zn alloy foams, but their comparisons are rare. Here we manufactured and comparatively characterized several Fe, Zn, and Mg alloys. The effects of several alloying elements on the biodegradation rate, corrosion rate, and mechanical properties of Mg, Fe and Zn alloys were investigated separately. One method to increase the biodegratation rate of Fe is the addition of biocompatible elements with lower electrode potential. The second method involves the addition of alloying elements to Fe in order to produce phases that induce galvanic corrosion and increase the corrosion rate. The results of this study revealed that Ti, Zn, Si, Fe, Mn, Mg, and TCP additions decrease the mechanical properties and increase the biodegradation rates of Fe alloys. The addition of Cu, Zn, Ti, Fe, Mn, and Si to Mg alloys increases their mechanical properties and decreases the biodegradation rates. The main disadvantage of zinc is its poor strength. It was shown that alloying with Fe, Mg, Ti, and Cu improves the strength of pure zinc. Si addition decreases the grain size of the alloy. Osseointegration and biocompatibility of Zn alloy are improved with TCP, Mg, and Ti. The introduction of Cu enhances antibacterial performance, strength, and ductility.

2. EXPERIMENTAL

2.1. Alloy Production

Zn, Fe, and Mg alloy foams were fabricated using irregularly shaped elemental iron, zinc, and magnesium powders with 99.9% purity (Alfa Aesar, USA). Copper, silicon, titanium, manganese, and TCP (tricalcium phosphate) powders with 99.9% purity (Alfa Aesar, USA) were used as alloying elements for Mg, Fe, and Zn alloys. The alloying metal powder additions were 5 wt %, and the TCP powder addition was 1 wt %. The average particle size of the powders was about 30–40 μm. First, the elemental metal powder mixtures were ball-milled (mechanical alloying) with zirconia balls (3 mm diameter) for 6–7 hours with a rotational speed of 400 rpm. The metal powder to zirconia ball ratio was ten to one. Highly porous Zn, Fe, and Mg alloy samples were fabricated by the powder metallurgy based space holder method. Carbamide (urea) powder in the range of 710–1000 μm was used as a pore former (Merck, Germany). The mean particle size of carbamide was 800–900 μm. The binder for green part was polyvinylalcohol (PVA). Mixtures were pressed at about 190–200 MPa into cylindrical samples with diameters of 20 and 12 mm and heights of 15–17 mm. Carbamide was removed in water and then the samples were sintered for 1 hour under vacuum. The sintering temperatures were 350, 520, and 1200°C for Zn, Mg, and Fe alloy samples, respectively.

2.2. Characterization of Mechanical Properties and Microstructure

Microstructure of sintered Zn, Mg, and Fe alloy samples was examined by scanning electron microscopy (FEI Quanta FEG 450).

2.3. Electrochemical Corrosion and Biodegradation Tests

Simulated body fluid (SBF) solution was prepared from chemicals (Merck, Germany) according to the literature [22]. The amounts of chemicals (in g/L) were 8.0NaCl, 0.3$CaCl_2$, 0.2KCl, 0.3$MgCl_2$, 0.2K_2HPO_4, 0.35$NaHCO_3$, 0.07Na_2SO_4, 6.0 tris, and 1.0 M HCl. The pH of the SBF solution was 6.60. Electrochemical corrosion tests were done with a potentiostat (Interface, Gamry). The test results were evaluated using software Gamry Framework. Initially, the open circuit potential (OCP) was analyzed. Tafel and linear polarization resistance tests were conducted to determine the corrosion rates.

Zn, Mg, and Fe alloy samples were dipped into the simulated body fluid (SBF) solution at room temperature for biodegradation tests. The solution volume to sample surface area ratio was constant. The volume of SBF solution was 50 mL. Samples with 70% porosity were machined, polished, and washed. The total porosity and surface area values of the samples were equal in the static immersion tests. Then the samples were exposed to saliva solution (50 mL) in closed polyethylene bottles. Foams with equal porosity levels were immersed in solution at

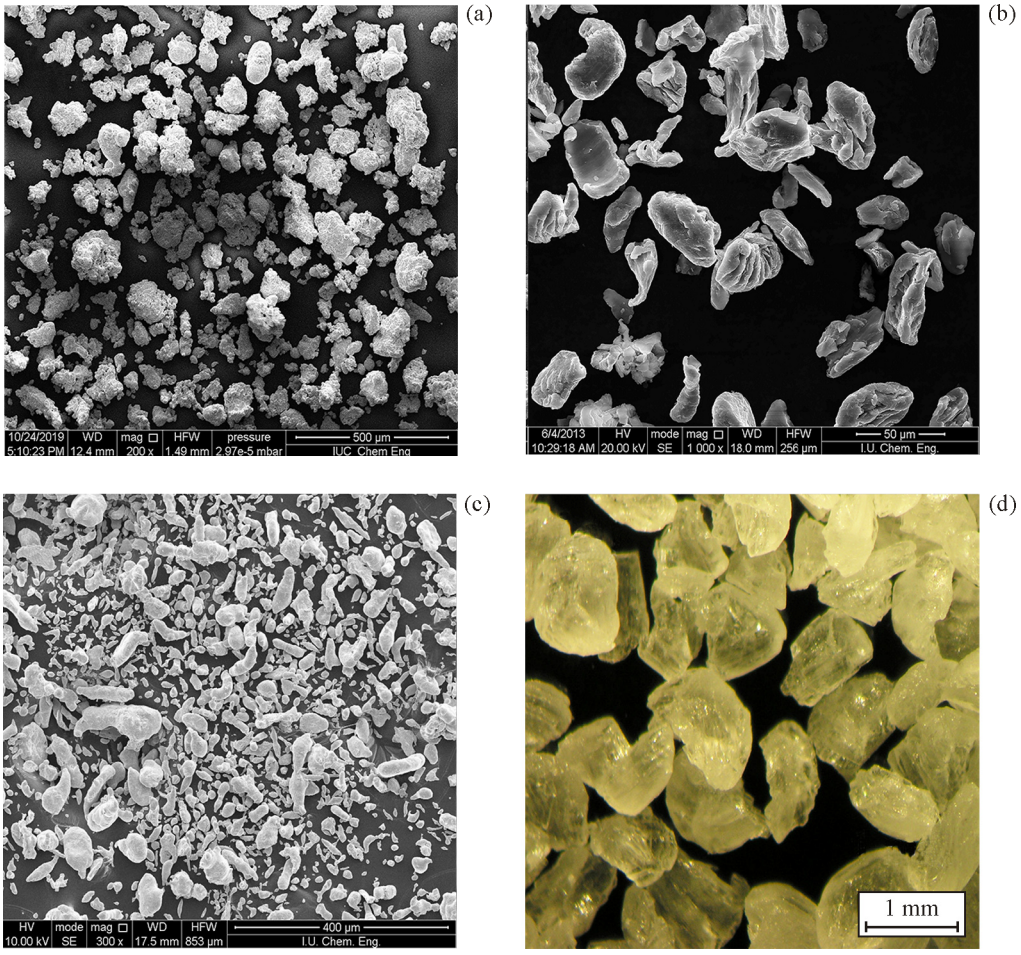

Fig. 1. SEM images of Fe (a), Mg (b), Zn (c), and carbamide powders (d).

room temperature for several soaking times. A solution without a sample was used for blank test. The area of pores was subtracted from the total surface area of foams to find the actual solid surface area. The weight loss values (%) of the samples were determined by the gravimetric (geometrical) method. After different times, the samples were removed from the solution. The weight loss (%) was computed by weighting the dried samples. An inductively coupled plasma-mass spectrometer (ICP-MS) (Thermo Scientific Elemental X Series 2) device was used to determine the metal ion release in the SBF solution.

3. RESULTS AND DISCUSSION

3.1. Microstructure Characterization

Biodegradable and biocompatible highly porous Zn, Fe, and Mg alloy samples were fabricated for temporary implant applications. Figure 1 illustrates the scanning electron microscopy (SEM) images of irregularly shaped powders of Fe, Mg, Zn, and pore former (carbamide).

The surface images of sintered highly porous Fe, Zn, and Mg samples are shown in Fig. 2. It is clear from the figure that there is an appropriate bonding between metal particles.

The general and cross-sectional views of sintered porous Fe, Zn, and Mg alloy samples are shown in Fig. 3. As one can see, there are no micro- and macrocracks on the sample surfaces. Pores are mainly interconnected and pore distributions are uniform in the foams. The biodegradable Fe, Zn, and Mg alloy foams were produced by the powder metallurgy based space holder method, which provides open porous structure. Open porosity enhances the osseointegration of bioinert metals. Tissue grows inside open pores and enhances bone–implant integration. In addition, open pores transmit body fluids. An increase in porosity decreases the elastic modulus of implants, which must be close to bone in order to prevent stress

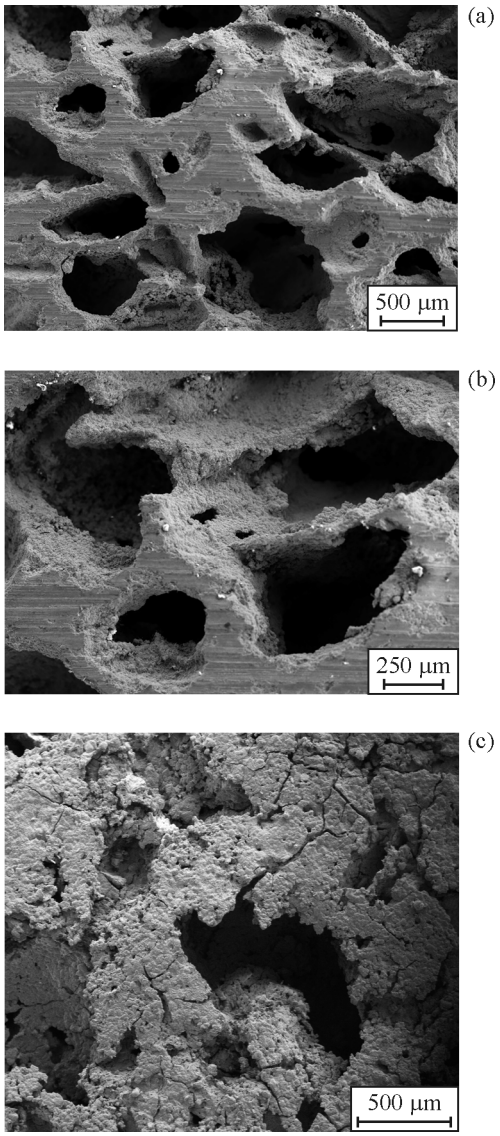

Fig. 2. SEM surface images of porous Fe (a), Zn (b) and Mg foams (c).

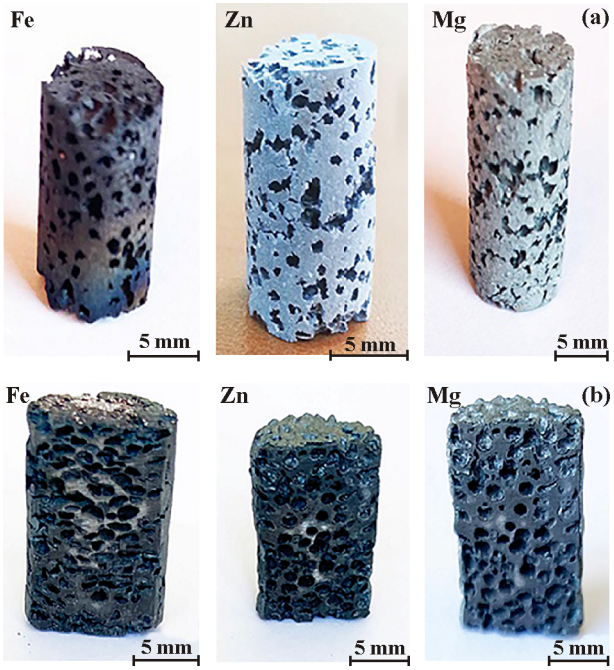

Fig. 3. Photographs of sintered porous Fe, Zn, and Mg samples: general view (a), cross-sectional view (b).

shielding. Powder metallurgy is suitable for the production of porous open-cell materials. Wide metal alloy compositions can be obtained by powder metallurgy with mechanical alloying. In addition, this method is free from solid solubility limitations.

Figure 4 illustrates the corrosion rate values of Zn alloys. In general, the corrosion rates calculated from the in vitro corrosion tests in SBF solution can be employed for estimating the in vivo biodegradation rates. The Pourbaix diagram of zinc illustrates that the surface oxide of zinc is not stable in acidic solutions. In neutral or alkaline conditions, Zn can be passivated. Zinc is highly active metal that dissolves in aqueous solutions. The addition of alloying elements can control the corrosion rate and corrosion products in zinc alloys. The corrosion properties of zinc alloys are associated with the precipitates and secondary phases, which are cathodic sites during biodegradation. As seen in Fig. 4, the maximum electrochemical corrosion rates were achieved in Zn-TCP and Zn-Mg samples, while the minimum corrosion rates were in Zn-Fe, Zn-Ti, and Zn-Cu alloys. The effect of Si addition on the corrosion rate of Zn was negligible. The corrosion rate of pure Zn was found to be similar to the literature data reported in [9–14, 23]. The corrosion rate value of novel biodegradable Zn-TCP foam is suitable for temporary hard tissue implant applications. The corrosion rate of novel biodegradable Zn-Ti

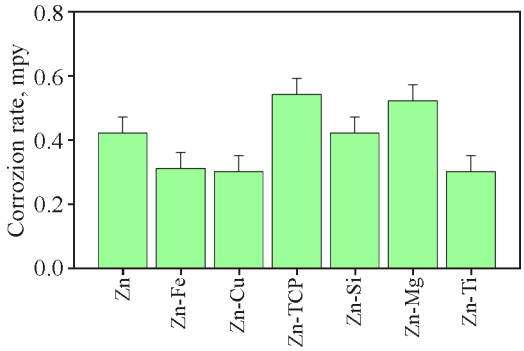

Fig. 4. Corrosion rate values of porous Zn alloys (color online).

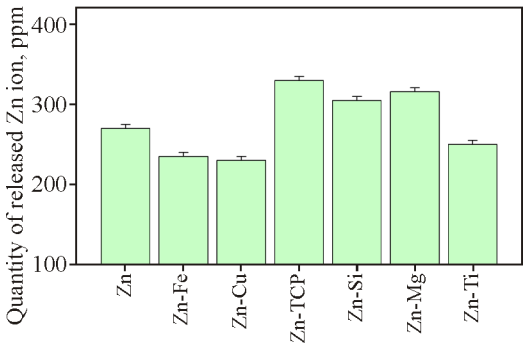

Fig. 5. Zn ion release values for porous Zn alloys (color online).

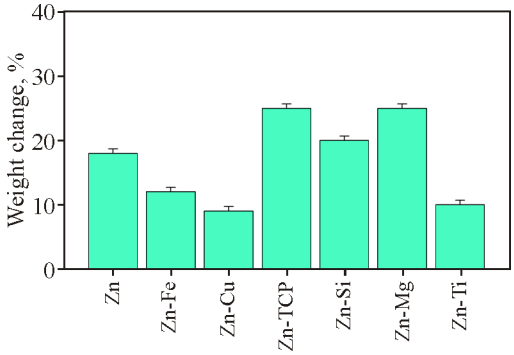

Fig. 6. Weight change values of porous Zn alloys (color online).

alloy is slightly lower than that of pure Zn. Ti addition decreased the electrochemical corrosion rate of Zn.

The Pourbaix diagram for Zn shows that no surface oxides of Zn are stable in an acidic environment (urine), while under neutral or slightly alkaline conditions (blood plasma) zinc has a tendency to passivate. The stability of both $Zn(OH)_2$ and ZnO is limited by the environmental parameters, including the presence of hydrogen, carbonates/bicarbonates and phosphates, chloride ions, and changes in the concentration of corrosion products. Furthermore, depending on the environmental parameters, other Zn compounds can be formed. In the presence of chloride ions, Zn may be able to form various soluble species and can lead to the formation of the main product of zinc hydroxychloride. The corrosion of pure Zn depends more on the properties of Zn itself, while the corrosion of Zn alloys is related to the size, distribution, and fraction of secondary phases. Differences in the corrosion rates are ascribed to the presence of secondary phases such as Mg_2Zn_{11}, $CaZn_{13}$, $SrZn_{13}$, $FeZn_{13}$, $AgZn_3$, etc. Zinc demonstrates high chemical activity, with an electrode potential (–0.76 V) falling between Mg (–2.37 V) and Fe (–0.44 V). Pure zinc exhibits moderate degradation rates (faster than slowly degrading Fe, but slower than rapidly degrading Mg) due to passive layers of moderate stability formed by corrosion products [24–28].

Figures 5 and 6 show the metal (Zn^{2+}) ion release and weight change (loss) values of highly porous Zn alloys for 21 days of immersion in SBF environment. In general, the metal (Zn^{2+}) ion release and weight loss values increased with time in the static immersion tests. The precipitates (corrosion products) consisted of zinc oxide (ZnO), zinc hydroxide ($Zn(OH)_2$), and calcium phosphates. The metal (Zn^{2+}) ion release amount was lower than the daily upper limit of 40 mg/day for zinc. The low metal release of Zn alloys is attributed to the surface oxide (ZnO). This surface oxide also prevents the diffusion of dissolved oxygen [1]. As seen from Fig. 5, the maximum ion release values were observed in Zn-TCP and Zn-Mg samples, while the minimum ion release was in Zn-Fe and Zn-Cu samples. The effect of Si and Ti additions on the metal ion release values was not high. The maximum weight change was observed in Zn-TCP and Zn-Mg samples, while the minimum weight change was in Zn-Cu sample. Studies on the metal ion release behavior of Zn-TCP, Zn-Si, and Zn-Ti are not available in the literature.

Figure 7 illustrates the Young's modulus variation of highly porous Zn alloys with immersion time in SBF. It can be seen that the Young's modulus values of highly porous Zn alloys decreased with immersion time. The main disadvantage of Zn is its poor strength. Alloying with Fe, Mg, Ti, and Cu improves the strength of pure Zn. Si addition reduced the grain size of the alloy. Osseointegration and biocompatibility of Zn alloy were improved with TCP, Mg, and Ti. The addition of Cu provided antibacterial performance, strength, and ductility. As seen from Fig. 7, the maximum elastic (Young's) modulus values were in

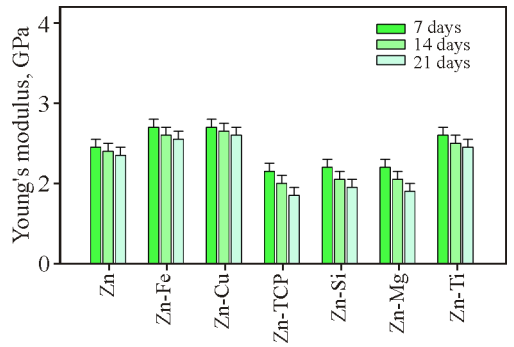

Fig. 7. Variation of Young's modulus of porous Zn alloys with immersion time (color online).

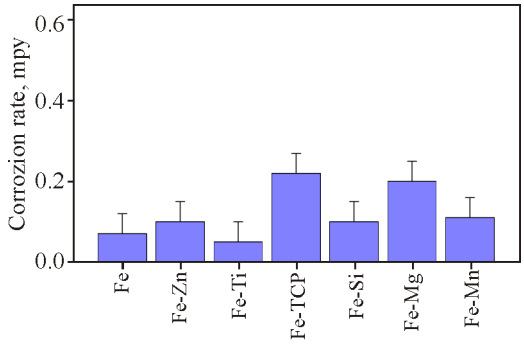

Fig. 8. Corrosion rate values of porous Fe alloys (color online).

Zn-Cu and Zn-Fe samples, while the minimum Young's modulus was in Zn-TCP, Zn-Si, and Zn-Mg samples. Cu and Fe additions increased the mechanical properties of Zn by solid solution strengthening. As seen from Fig. 7, the decrease in the elastic (Young's) modulus values of the samples was about 10–15% in 21 days.

Biodegradable metals must show mechanical properties close to bone, a biodegradation rate close to the tissue healing rate, and high biocompatibility. Open porous structure is important in implants for vascularization and tissue ingrowth. Open-cell foams can be manufactured by powder metallurgy. Sadighikia et al. [9] manufactured Zn foams with open-cell microstructure by powder metallurgy using carbamide as a pore former. Azizi et al. [10] used powder metallurgy to produce Zn-Al-Cu alloy. Berent et al. [13] studied cast eutectic Zn-Al-Si alloy and showed that the addition of Si to Zn-Al alloys increases the mechanical properties. Kafri et al. [14] studied Zn-Fe alloy for biodegradable implants. Fe was used as an alloying element in order to adjust the biodegradation rate due to the micro-galvanic effect produced by secondary phases. Zn-Fe alloy samples were manufactured by casting. The corrosion rate of Zn-Fe alloy samples was higher than that of pure Zn. Qu et al. [23] studied biodegradable Zn-Cu alloys. They found that Zn-Cu alloy shows antibacterial activity by inhibiting pathogen adhesion and biofilm formation. Zn-2Cu alloy had the best mechanical properties, biocompatibility, and osteogenic properties. The findings indicated that Zn-2Cu alloy can inhibit both coagulase-positive and coagulase-negative as well as antibiotic-resistant strains by preventing biofilm formation. The group treated with Zn-2Cu alloy showed antibacterial activity, lower inflammatory and toxic side effects, and reduced bone loss. Shi et al. [29] studied the optimization of Fe addition in Zn through second phase refinement. The authors used Zn-0.3Fe alloy suffered from coarse $FeZn_{13}$ second phase particles as a touchstone to testify the effect of microstructure refinement via rapid solidification and multipass rolling. The size of $FeZn_{13}$ particles decreased from 24 to 2 μm, and Zn grains were refined to 5 μm. The results showed that microstructure refinement improves the mechanical and biodegradation properties of Zn alloys.

Tong et al. [30] studied the biodegradation rate, antibacterial properties, and cytotoxicity of Zn-Cu alloy foams (Zn-3Cu, Zn-3.5Cu, Zn-11Cu) with 54–77% porosity for bone implant applications. Shi et al. [31] studied $FeZn_{13}$ intermetallic compounds (main second phase) in biodegradable Fe-containing Zn alloys (Zn-Fe, Zn-Mn-Fe, Zn-Cu-Fe). Lin et al. [32] produced and studied biodegradable Zn-1.0Cu-0.1Ti alloy with antibacterial properties for implant applications. The microstructure of Zn-1Cu-0.1Ti alloy was composed of a η-Zn matrix phase, an intermetallic compound $TiZn_{16}$ phase, and an ε-$CuZn_5$ phase. Most of the intermetallic compound $TiZn_{16}$ phase was distributed along the grain boundaries.

Figure 8 presents the electrochemical corrosion rate values of Fe alloys. The corrosion rate of Fe-TCP and Fe-Mg samples was relatively high. The corrosion rate of Fe-Ti sample was lower than for pure Fe. As seen from the figure, the addition of Si, Zn, and Mn elements also increased the corrosion rate of Fe alloy samples.

Figures 9 and 10 show the metal (Fe^{2+}) ion release and weight change (loss) values of highly porous Fe alloys for 21 days of immersion in SBF solution. It can be seen that the metal (Fe^{2+}) ion release and weight loss values increased with time in the static immersion tests. The amount of metal ion release was lower than the daily upper limit for iron (Fe^{2+}). The maximum metal ion release values were observ-

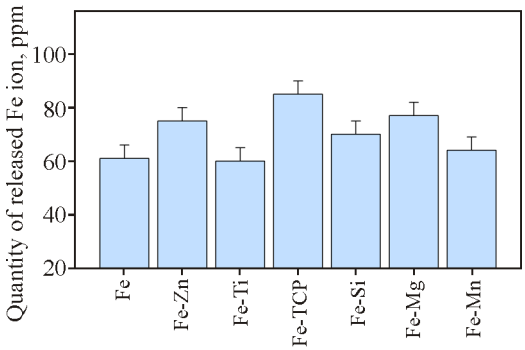

Fig. 9. Fe ion release values for porous Fe alloys (color online).

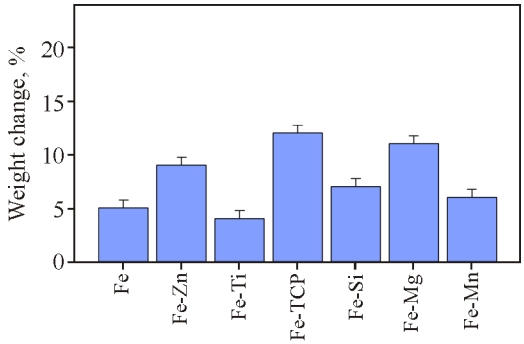

Fig. 10. Weight change values of porous Fe alloys (color online).

ed in Fe-TCP and Fe-Mg samples, while the minimum metal ion release was in Fe-Ti alloy. The maximum weight change was in Fe-TCP and Fe-Mg samples, and the minimum one was in Fe-Ti sample.

Figure 11 illustrates the Young's modulus variation of highly porous Fe alloys with immersion time in SBF. The data indicate that the Young's modulus values of highly porous Fe alloys decreased with immersion time. One method to increase the biodegradation rate of Fe is the addition of biocompatible elements with lower standard electrode potential. The second method involves the addition of alloying elements to Fe in order to produce phases that induce galvanic corrosion and increase the corrosion rate. In the present study, Ti, Zn, Si, Mn, Mg, and TCP additions decreased the mechanical properties and increased the biodegradation rates of Fe alloys. According to Fig. 11, the maximum elastic (Young's) modulus values were achieved in Fe-Zn and pure Fe samples, while the minimum elastic (Young's) modulus was in Fe-TCP and Fe-Mg samples. TCP and Mg additions reduced the mechanical properties of Fe due to their low strength. The decrease in the

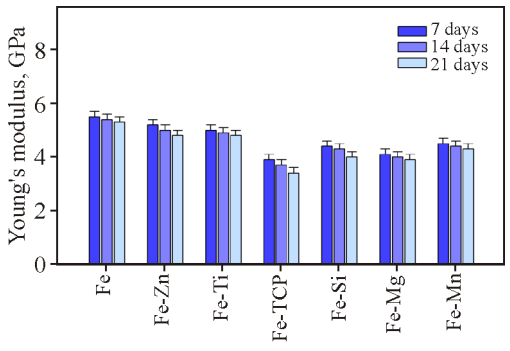

Fig. 11. Variation of Young's modulus of porous Fe alloys with immersion time (color online).

Young's modulus values of the samples was about 8–10% in 21 days.

Francis et al. [19] studied Fe alloys for stent applications. It was shown that implants based on Fe alloys show high strength, corrosion rate, and biocompatibility. Fe alloy stents may biodegrade slowly while retaining their mechanical integrity. Orinakova et al. [20] produced iron alloy foams by the replication method using foamed polyurethane. Capek et al. [21] produced Fe foams by powder metallurgy using ammonium bicarbonate as a pore former. Gasior et al. [33] examined biodegradable iron alloys. They concluded that some of the methods of obtaining ferrous biomaterials such as spark plasma sintering and vacuum induction melting should be abandoned. Other methods such as vacuum arc melting and electroforming should be reconsidered once again. Powder metallurgy and template-based synthesis of porous systems have the potential to produce degrading iron-based systems. Further work is needed to achieve desired iron-based systems and to find new phase additions for iron, taking into account that some degradation products may lead to negative side effects. In the case of pure iron, the focus should be placed on optimizing the degradation rate related to morphology, excluding the influence of other elements. Sotoudehbagha et al. [34] discussed antibacterial biodegradable Fe-Mn-Ag alloys produced by powder metallurgy. Various compositions and synthesis methods of biodegradable iron alloys were considered aiming for temporary implants. Fe-30Mn-(1-3)Ag alloys were synthesized by powder metallurgy and assessed for their microstructure, mechanical properties, corrosion rate, antibacterial activity, and cytotoxicity. Alloy with 3 wt % Ag displayed the highest density, strength, and corrosion rate. Optimal cytotoxicity and antibacterial activity were reached by addition of 1 wt % Ag. Hermawan et al. [35] studied Fe-Mn alloys for biodegradable stents. The biodegradation products of Fe-Mn alloys consisted of metal hydroxides and calcium/phosphorus layers. The alloys showed low inhibition with respect to fibroblast cells. Liu et al. [36] studied Fe-Mn-Ag alloys as biodegradable metals. Biodegradable pure Fe, Fe-30Mn, and Fe-30Mn-Ag alloys were produced by rapid solidification. A fine alpha-Fe dendrite was formed in Fe, resulting in a high strength. Fe-30Mn alloy with 1% Ag exhibited an increase in the biodegradation rate due to the precipitation of Ag-rich particles and microgalvanic corrosion. Fe-30Mn-Ag alloy also exhibited magnetic compatibility.

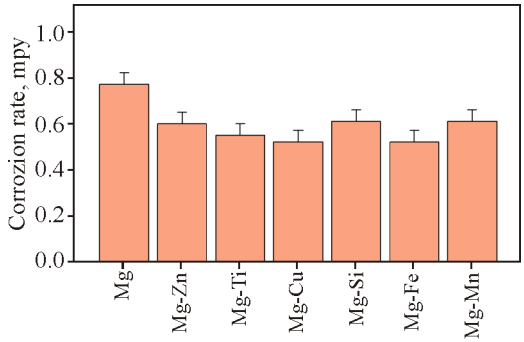

Fig. 12. Corrosion rate values of porous Mg alloys (color online).

Figure 12 presents the corrosion rate values of Mg alloys. One can see that the corrosion rate of pure Mg sample was relatively high. The corrosion rate values of Mg-Ti and Mg-Fe samples were lower.

Figures 13 and 14 show the metal (Mg^{2+}) ion release and weight change (loss) values of highly porous Mg alloys for 21 days of immersion in SBF solution. The metal (Mg^{2+}) ion release and weight loss values increased with time in the static immersion tests. The amount of metal ion release was lower than the daily upper limit for magnesium. The maximum metal ion release was observed in pure Mg and Mg-Zn samples, while the minimum ion release was in Mg-Cu and Mg-Fe samples. The maximum weight change was in pure Mg and Mg-Si, while the minimum one was in Mg-Cu and Mg-Fe.

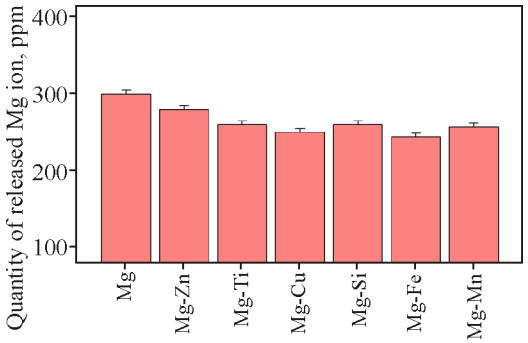

Fig. 13. Mg ion release values for porous Mg alloys (color online).

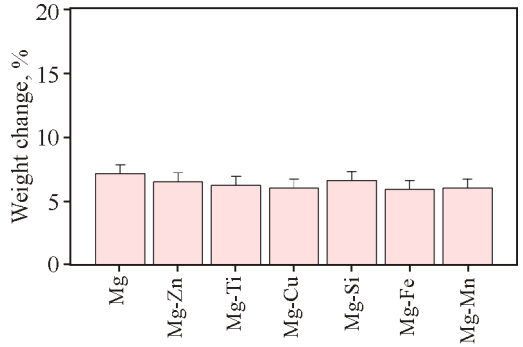

Fig. 14. Weight change values of porous Mg alloys (color online).

Figure 15 illustrates the Young's modulus variation of highly porous Mg alloys with immersion time in SBF environment. According to the diagram, the Young's modulus values of highly porous Mg alloys deceased with immersion time. Cu, Zn, Ti, Fe, Mn, and Si additions increased the mechanical properties and decreased the biodegradation rates of Mg alloys. The maximum elastic (Young's) modulus values were in Mg-Cu and Mg-Fe samples, and the minimum elastic moduli were in pure Mg and Mg-Si. Cu and Fe additions increased the mechanical properties of Mg by solid solution strengthening. Ti and Mn additions increased the mechanical properties of Mg at moderate level. The decrease in the Young's modulus values of the samples was about 30–40% in 21 days.

Seyedraoufin and Mirdamadi [2] prepared Mg-Zn scaffolds. According to their results, Mg-Zn alloy can be considered as a scaffold material. Porous Mg has potential as a biodegradable scaffold. Dissolved Mg ions may promote cell attachment and tissue growth. Bobe et al. [37] fabricated a biodegradable open-porous scaffold from Mg alloy by sintering. It was shown that the in vitro environment affects the corrosion rates compared with the in vivo environment. The composition of culture media affects the ionic composition of the extract by selectively dissolving ions. Aghion et al. [38] produced Mg foams by the space holder method as a scaffold. The amount and delivery time of the released drug were controlled by space holder. Wen et al. [39] produced Mg foams for scaffold applications. They investigated the mechanical properties of Mg with a poro-

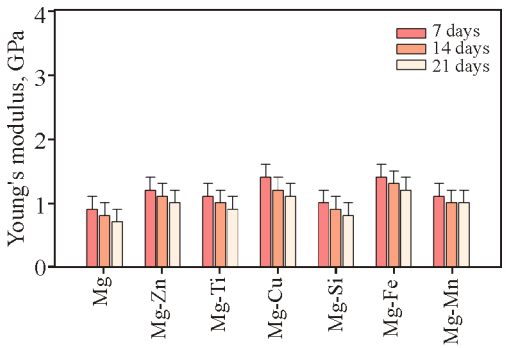

Fig. 15. Variation of Young's modulus of porous Mg alloys with immersion time (color online).

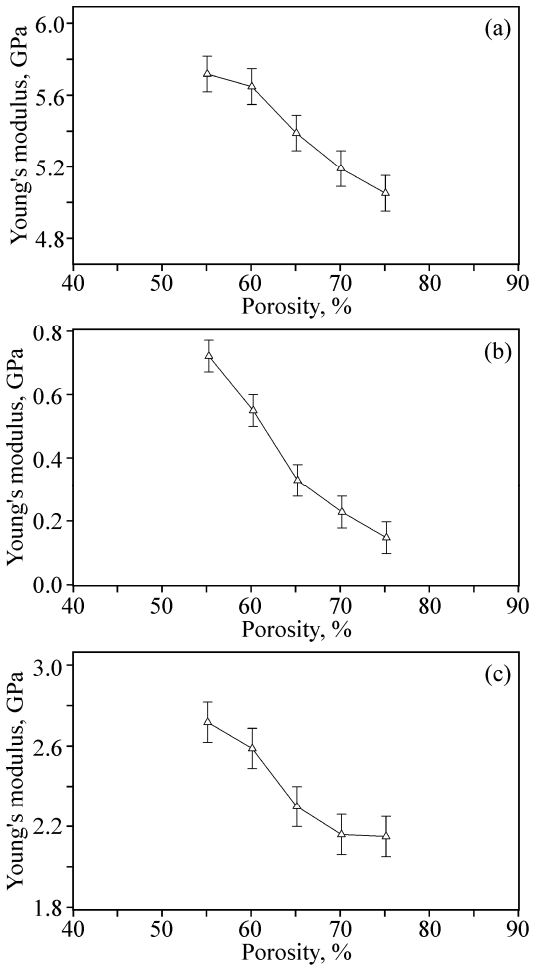

Fig. 16. Variation of Young's modulus of porous Fe (a), Mg (b) and Zn (c) alloys with porosity.

sity of 35–55% and a pore size of 70–400 μm. The results indicated that the elastic modulus of the material increases with decreasing porosity. The mechanical properties were close to bone. Erryani et al. [40] studied microstructures and mechanical properties of Mg alloy foam based on Mg-Zn-Ca-$CaCO_3$ system. The objective of the study was to characterize the microstructure and mechanical characteristics of Mg-Ca-Zn-$CaCO_3$ alloy as a porous implant material. $CaCO_3$ functioned as a foaming agent to produce gas bubbles. Mg-Ca-Zn-$CaCO_3$ alloy was produced by powder metallurgy with three compositions (96Mg-Ca-3Zn-$CaCO_3$, 91Mg-Ca-3Zn-5$CaCO_3$, 86Mg-Ca-3Zn-10$CaCO_3$). The mixed and milled powders were pressed at 200 MPa. Sintering was carried out at 650°C for 15 hours.

The curves of Young's modulus variation of sintered highly porous Fe, Mg, and Zn alloys are presented in Fig. 16. As seen from the figure, the elastic modulus of the samples decreased with increasing porosity. The Young's modulus values of sintered 70% porous Fe, Mg, and Zn alloys were respectively about 5.20, 0.24, and 2.15 GPa. The Young's moduli of sintered 70–75% porous Fe, Mg, and Zn alloys were close to bone. The final pore size of sintered Zn, Mg, and Fe alloy samples was also related to the pore former (carbamide) particle size. The mean particle size of carbamide was 800–850 μm, while the pore diameter of the sintered samples was 500–600 μm. The smaller pore sizes were attributed to crushing of the pore former during compaction. In general, the minimum requirement for the pore size is 100 μm due to cell migration and transport. With pores smaller than about 100 μm, cells do not grow into open pores because of pore clogging by huge cells [41].

Trivedi et al. [42] investigated the effect of the grain size on the mechanical properties of forged Mg-2Zn-2Gd alloy. As-cast and annealed samples were forged for 2 passes. Multiaxial forging reduced the grain size to 1 μm. When the samples were forged, the strength increased. The improvement in mechanical properties was attributed to the homogeneous structure, which resulted from grain fragmentation. Annealing also led to fine distribution of precipitates. Guan et al. [43] investigated Mg-Sn-Mn-La alloys strengthened by nanoscale precipitates. The authors explored the effect of La on the microstructure and mechanical properties of Mg-Sn-Mn-La alloy plates processed by rheo-rolling. At 0.2%, La dissolved in Mg. At a 0.6% La content, plate-shaped compounds (La_5Sn_3, Mg_2Sn, $Mg_{17}La_2$) were formed, which had a pinning effect.

4. CONCLUSIONS

In this study, highly porous biocompatible and biodegradable Zn, Fe, and Mg alloy foams were obtained for temporary implant and scaffold applications. Highly porous samples with interconnected porous structure were fabricated by the conventional powder metallurgy (press-sinter) based space holder method. Mg, Fe, and Zn are three main bioabsorable metals. Mg alloys biodegrade too fast with H_2 evolution. The biodegradation rate of Fe alloys is too slow, and by-products of Fe remain inside the body for a long time. Zn is also identified as a promising biodegradable metal along with Mg and Fe alloys. Zn alloys show biodegradation rates in the middle between Mg and Fe alloys (closer to the ideal values), and their biodegradation by-products are mainly bioresorbable. Here we produced and characterized several Fe, Zn, and Mg alloys. The effects of alloying

elements on biodegradation, corrosion, and mechanical properties were investigated separately. Since the mechanical properties of temporary hard tissue implants must decrease slowly, the variation of mechanical properties with time in the foams was investigated. Electrochemical corrosion tests of the samples were conducted in a simulated body fluid (SBF) solution. The biodegradation behavior of sintered Mg, Zn, and Fe alloy samples was investigated by weight loss and metal ion release measurements after immersion in SBF solution. Fe^{2+}, Zn^{2+}, and Mg^{2+} ion release amounts were negligible compared with the daily recommended limit for humans according to the experimental data. Ti, Zn, Si, Fe, Mn, Mg, and TCP additions decreased the mechanical properties and increased the biodegradation rates of Fe alloys. Cu, Zn, Ti, Fe, Mn, and Si additions increased the mechanical properties and decreased the biodegradation rates of Mg alloys. The main disadvantage of Zn is its poor strength. It was shown that alloying with Fe, Mg, Ti, and Cu improves the strength of pure Zn. Si addition decreases the grain size of the alloy. Osseointegration and biocompatibility of Zn alloy was improved with TCP, Mg, and Ti. The addition of Cu provided antibacterial performance, strength, and ductility.

FUNDING

This work was partially supported by the Scientific Research Projects Coordination Unit of Istanbul University-Cerrahpasa, Projects Nos. 35659, 35660, 35175.

REFERENCES

1. Zhao, L., Zhang, Z., Song, Y., Liu, S., Qi, Y., Wang, X., Wang, Q., and Cui, C., Mechanical Properties and In Vitro Biodegradation of Newly Developed Porous Zn Scaffolds for Biomedical Applications, *Mater. Design*, 2016, vol. 108, pp. 136–144. https://doi.org/10.1016/j.matdes.2016.06.080
2. Seyedraoufin, Z.S. and Mirdamadi, S., Synthesis, Microstructure and Mechanical Properties of Porous Mg-Zn Scaffolds, *J. Mech. Behav. Biomed. Mater*., 2013, vol. 21, pp. 1–8. http://dx.doi.org/10.1016/j.jmbbm.2013.01.023
3. Li, H., Peng, Q., Li, X., Li, K., Han, Z., and Fang, D., Microstructures, Mechanical and Cytocompatibility of Degradable Mg–Zn Based Orthopedic Biomaterials, *Mater. Design*, 2014, vol. 58, pp. 43–51. https://doi.org/10.1016/j.matdes.2014.01.031
4. Yang, H., Wang, C., Liu, C., Chen, H., Wu, Y., Han, J., Jia, Z., Lin, W., Zhang, D., Li, W., Yuan, W., Guo, H., Li, H., Yang, G., Kong, D., Zhu, D., Takashima, K., Ruan, L., Nie, J., Li, X., and Zheng, Y., Evolution of the Degradation Mechanism of Pure Zinc Stent in the One-Year Study of Rabbit Abdominal Aorta Model, *Biomaterials*, 2017, vol. 145, pp. 92–105. https://doi.org/10.1016/j.biomaterials.2017.08.022
5. Vojtech, D., Kubasek, J., Serak, J., and Novak, P., Mechanical and Corrosion Properties of Newly Developed Biodegradable Zn-Based Alloys for Bone Fixation, *Acta Biomater*., 2011, vol. 7, pp. 3515–3522. https://doi.org/10.1016/j.actbio.2011.05.008
6. Zhao, S., Seitz, J.M., Eifler, R., Maier, H.J., Guillory II, R.J., Earley, E.J., Drelich, A., Goldman, J., and Drelich, J.W., Zn-Li Alloy after Extrusion and Drawing: Structural, Mechanical Characterization, and Biodegradation in Abdominal Aorta of Rat, *Mater. Sci. Eng. C*, 2017, vol. 76, pp. 301–312. https://doi.org/10.1016/j.msec.2017.02.167
7. Bowen, P.K., Guillory II, R.J., Shearier, E.R., Seitz, J.M., Drelich, J., Bocks, M., Zhao, F., and Goldman, J., Metallic Zinc Exhibits Optimal Biocompatibility for Bioabsorbable Endovascular Stents, *Mater. Sci. Eng. C*, 2015, vol. 56, pp. 467–472. https://doi.org/10.1016/j.msec.2015.07.022
8. Drelich, A.J., Zhao, S., Guillory II, R.J., Drelich, J.W., and Goldman, J., Long-Term Surveillance of Zinc Implant in Murine Artery: Surprisingly Steady Biocorrosion Rate, *Acta Biomater*., 2017, vol. 58, pp. 539–549. https://doi.org/10.1016/j.actbio.2017.05.045
9. Sadighikia, S., Abdolhosseinzadeh, S., and Asgharzadeh, H., Production of High Porosity Zn Foams by Powder Metallurgy Method, *Powder Met*., 2015, vol. 58, no. 1, pp. 61–66. https://doi.org/10.1179/1743290114Y.0000000109
10. Azizi, A. and Haghighi, G.G., Fabrication of ZAMAK 2 Alloys by Powder Metallurgy Process, *Int. J. Adv. Manuf. Technol*., 2015, vol. 77, pp. 2059–2065. https://doi.org/10.1007/s00170-014-6611-z
11. Gulsoy, H.O. and German, R.M., Production of Micro-Porous Austenitic Stainless Steel by Powder Injection Molding, *Scripta Mater*., 2008, vol. 58, pp. 295–298. https://doi.org/10.1016/j.scriptamat.2007.10.004
12. Kafkas, F. and Ebel, T., Metallurgical and Mechanical Properties of Ti-24Nb-4Zr-8Sn Alloy Fabricated by Metal Injection Molding, *J. Alloy. Compnd*., 2014, vol. 617, pp. 359–366. https://doi.org/10.1016/j.jallcom.2014.07.168
13. Berent, K., Pstrus, J., and Gancarz, T., Thermal and Microstructure Characterization of Zn-Al-Si Alloys and Chemical Reaction with Cu Substrate during Spreading, *J. Mater. Eng. Perform*., 2016, vol. 25, pp. 3375–3383. https://doi.org/10.1007/s11665-016-2074-8
14. Kafri, A., Ovadia, S., Goldman, J., Drelich, J., and Aghion, E., The Suitability of Zn–1.3%Fe Alloy as a Biodegradable Implant Material, *Metals*, 2018, vol. 8, p. 153. https://doi.org/10.3390/met8030153
15. Yang, D., Chen, J., Chen, W., Wang, L., Wang, H., Jiang, J., and Ma, A., Fabrication of Cellular Zn–Mg

Alloy Foam by Gas Release Reaction Via Powder Metallurgical Approach, *J. Mater. Sci. Technol*., 2017, vol. 33, pp. 1141–146. https://doi.org/10.1016/j.jmst.2017.03.019
16. Wang, Y.H., Xiao, L.R., Zhao, X.J., Zhang, W., Song, Y.F., Guo, L., and Wang, Y., Corrosion Behavior of Zn-Cu-Ti and Zn-Cu-Ti-Mg Alloys in NaCl Solution, *Mater. Corros*., 2016, vol. 67, no. 3, pp. 297–304. https://doi.org/10.1002/maco.201508410
17. Tang, Z., Huang, H., Niu, J., Zhang, L., Zhang, H., Pei, J., Tan, J., and Yuan, G., Design and Characterizations of Novel Biodegradable Zn-Cu-Mg Alloys for Potential Biodegradable Implants, *Mater. Design*, 2017, vol. 117, pp. 84–94. https://doi.org/10.1016/j.matdes.2016.12.075
18. Zheng, Y.F., Gu, X.N., and Witte, F., Biodegradable Metals, *Mater. Sci. Eng. R*, 2014, vol. 77, pp. 1–34. https://doi.org/10.1016/j.mser.2014.01.001
19. Francis, A., Yang, Y., Virtanen, S., and Boccaccini, A.R., Iron and Iron Based Alloys for Temporary Cardiovascular Applications, *J. Mater. Sci. Mater. Med*., 2015, vol. 26, p. 138.
20. Orinakova, R., Orinak, A., Buckova, L.M., Giretova, M., Medvecky, L., Labbanczova, E., Kupkova, M., Hrubovcakova, M., and Kova, K., Iron Based Degradable Foam Structures for Potential Orthopedic Applications, *Int. J. Electrochem. Sci*., 2013, vol. 8, pp. 12451–12465.
21. Capek, J., Vojtech, D., and Oborna, A., Powder Metallurgical Techniques for Fabrication of Biomaterials, *Mater. Design*, 2015, vol. 83, pp. 468–482. https://doi.org/10.21062/ujep/x.2015/a/1213-2489/MT/15/6/964
22. Kokubo, T. and Takadama, H., How Useful is SBF in Predicting In Vivo Bone Bioactivity? *Biomaterials*, 2007, vol. 27, pp. 2907–2915. https://doi.org/10.1016/j.biomaterials.2006.01.017
23. Qu, X., Yang, H., Jia, B., Yu, Z., Zheng, Y., and Dai, K., Biodegradable Zn-Cu Alloys Show Antibacterial Activity Against MRSA Bone Infection by Inhibiting Pathogen Adhesion and Biofilm Formation, *Acta Biomater*., 2020, vol. 117, pp. 400–417. https://doi.org/10.1016/j.actbio.2020.09.041
24. Mostaed, E., Sikora-Jasinska, M., Drelich, J.W., and Vedani, M., Zinc-Based Alloys for Degradable Vascular Stent Applications, *Acta Biomater*., 2018, vol. 71, pp. 1–23. https://doi.org/10.1016/j.actbio.2018.03.005
25. Yang, H., Qu, X., Lin, W., Wang, C., Zhu, D., Dai, K., and Zheng, Y., In Vitro and İn Vivo Studies on Zinc-Hydroxyapatite Composites as Novel Biodegradable Metal Matrix Composite for Orthopedic Applications, *Acta Biomater*., 2018, vol. 71, pp. 200–214. https://doi.org/10.1016/j.actbio.2018.03.007
26. Champagne, S., Mostaed, E., Safizadeh, F., Ghali, E., Vedani, M., and Hermawan, H., In Vitro Degradation of Absorbable Zinc Alloys in Artificial Urine, *Materials*, 2019, vol. 12, p. 295. https://doi.org/10.3390/ma12020295
27. Shi, Z.Z., Yu, J., Liu, X.F., and Wang, L.N., Fabrication and Characterization of Novel Biodegradable Zn-Mn-Cu Alloys, *J. Mater. Sci. Technol*., 2018, vol. 34, pp. 1008–1015. https://doi.org/10.1016/j.jmst.2017.11.026
28. Liu, Z., A New Approach Toward Designing and Synthesizing the Microalloying Zn Biodegradable Alloys with Improved Mechanical Properties, *Metall. Mater. Trans. A*, 2019, vol. 50, pp. 311–325. https://doi.org/10.1007/s11661-018-4978-4
29. Shi, Z., Li, C., Li, M., Li, X., and Wang, L., Second Phase Refining Induced Optimization of Fe Alloying in Zn: Significantly Enhanced Strengthening Effect and Corrosion Uniformity, *Int. J. Min. Metall. Mater*., 2022, vol. 29, no. 4, p. 796. https://doi.org/10.1007/s12613-022-2468-6
30. Tong, X., Shi, Z., Xu, L., Lin, J., Zhang, D., Wang, K., Li, Y., and Wen, C., Degradation Behavior, Cytotoxicity, Hemolysis, and Antibacterial Properties of Electro-Deposited Zn–Cu Metal Foams as Potential Biodegradable Bone Implants, *Acta Biomater*., 2020, vol. 102, no. 4, pp. 81–92. https://doi.org/10.1016/j.actbio.2019.11.031
31. Shi, Z.Z., Gao, X.X., and Liu, X.F., $FeZn_{13}$ Intermetallic Compound in Biodegradable Znfe Alloy: Twinning and Its Shape Effect, *Mater. Character*., 2020, vol. 164, p. 110352. https://doi.org/10.1016/j.matchar.2020.110352
32. Lin, J., Tong, X., Shi, Z., Zhang, D., Zhang, L., Wang, K., Wei, A., Jin, L., Lin, J., Li, Y., and Wen, C., A Biodegradable Zn-1Cu-0.1Ti Alloy with Antibacterial Properties for Orthopedic Applications, *Acta Biomater*., 2020, vol. 106, pp. 410–427. https://doi.org/10.1016/j.actbio.2020.02.017
33. Gasior, G., Szczepanski, J., Radtke, A., Biodegradable Iron-Based Materials-What Was Done and What More Can Be Done? *Materials*, 2021, vol. 14, p. 3381. https://doi.org/10.3390/ma14123381
34. Sotoudehbagha, P., Sheibani, S., Khakbiz, M., Barough, S.E., and Hermawan, H., Novel Antibacterial Biodegradable Fe-Mn-Ag Alloys Produced by Mechanical Alloying, *Mater. Sci. Eng. C*, 2018, vol. 88, pp. 88–94. https://doi.org/10.1016/j.msec.2018.03.005
35. Hermawan, H., Purnama, A., Dube, D., Couet, J., and Mantovani, D., Fe-Mn Alloys for Metallic Biodegradable Stents: Degradation and Cell Viability Studies, *Acta Biomater*., 2010, vol. 6, pp. 1852–1860. https://doi.org/10.1016/j.actbio.2009.11.025
36. Liu, R.Y., He, R.G., Xu, L.Q., and Guo, S.F., Design of Fe–Mn–Ag Alloys as Potential Candidates for Biodegradable Metals, *Acta Metall. Sin. (Engl. Lett.)*, 2018, vol. 31, pp. 584–590. https://doi.org/10.1007/s40195-018-0702-z
37. Bobe, K., Willbold, E., Morgenthal, I., Andersen, O., Studnitzky, T., Nellesen, J., Tillmann, W.C., Vogt, K., Vano, and Witte, F., In Vitro and In Vivo Evaluation of Biodegradable, Open-Porous Scaffolds Made of

Sintered Magnesium W4 Short Fibres, *Acta Biomater*., 2013, vol. 9, pp. 8611–8623 https://doi.org/10.1016/j.actbio.2013.03.035
38. Aghion, E., Yered, T., Perez, Y., and Gueta, Y., The Prospects of Carrying and Releasing Drugs Via Biodegradable Magnesium Foam, *Adv. Eng. Mater*., 2010, vol. 12, no. 8, pp. 374–379. https://doi.org/10.1002/adem.200980044
39. Wen, C.E., Yamada, Y., Shimijima, K., Chino, Y., Hosokawa, Y.H., and Mabuchi, M., Porous Shape Memory Alloy Scaffolds for Biomedical Applications: A Review, *Mater. Lett*., 2004, vol. 58, pp. 357–360.
40. Erryani, A., Pramuji, F., Annur, D., Amal, M.I., and Kartika, I., Microstructures and Mechanical Study of Mg Alloy Foam Based on Mg-Zn-Ca-$CaCO_3$ System, *Mater. Sci. Eng*., 2017, vol. 202, p. 012028. https://doi.org/10.1088/1757-899X/202/1/012028
41. Ratner, B.D., Hoffman, A.S., Schoen, F.J., and Lemons, J.E., *Biomaterials Science: An Introduction to Materials in Medicine*, Elsevier, 2012.
42. Trivedi, P., Nune, K.C., and Misra, R.D.K., Grain Refinement to Submicron Regime in Multiaxial Forged Mg-2Zn-2Gd Alloy and Relationship to Mechanical Properties, *Mater. Sci. Eng. A*, 2016, vol. 668, pp. 59–65. https://doi.org/10.1016/j.msea.2016.05.050
43. Guan, R.G., Shen, Y.F., and Zhao, Z.Y., Nanoscale Precipitates Strengthened Lanthanum-Bearing Mg-3Sn-1Mn Alloys through Continuous Rheo-Rolling, *Sci. Rep. Nat*., 2016, vol. 6, pp. 23154:1–15. https://doi.org/10.1038/srep23154